Reexpression of caveolin-1 in endothelium rescues the vascular, cardiac, and pulmonary defects in global caveolin-1 knockout mice

Takahisa Murata, Michelle I. Lin, Yan Huang, Jun Yu, Phillip Michael Bauer, Frank J. Giordano, and William C. Sessa

Department of Pharmacology and Program in Vascular Cell Signaling and Therapeutics, Boyer Center for Molecular Medicine, Yale University School of Medicine, New Haven, CT 06511

Caveolin-1 (Cav-1) is the principal structural component of caveolae organelles in smooth muscle cells, adipocytes, fibroblasts, epithelial cells, and endothelial cells (ECs). Cav-1–deficient (Cav-1 knockout [KO]) mice are viable and show increases of nitric oxide (NO) production in vasculature, cardiomyopathy, and pulmonary dysfunction. In this study, we generated EC-specific Cav-1–reconstituted (Cav-1 RC) mice and reexamined vascular, cardiac, and pulmonary phenotypes. Cav-1 KO pulmonary arteries had decreased smooth muscle contractility and increased endothelial NO synthase activation and hypotension; the latter two effects were rescued completely in Cav-1 RC mice. Cav-1 KO mice exhibited myocardial hypertrophy, pulmonary hypertension, and alveolar cell hyperproliferation caused by constitutive activation of p42/44 mitogen-activated protein kinase and Akt. Interestingly, in Cav-1 RC mice, cardiac hypertrophy and pulmonary hypertension were completely rescued, whereas alveolar hyperplasia was partially recovered because of the lack of rescue of Cav-1 in bronchiolar epithelial cells. These results provide clear physiological evidence supporting the important role of cell type–specific Cav-1 expression governing multiple phenotypes in the vasculature, heart, and lung.

CORRESPONDENCE
William C. Sessa:
william.sessa@yale.edu

Abbreviations used: Ach, acetylcholine; cGMP, cyclic guanosine monophosphate; EC, endothelial cell; eNOS, endothelial NOS; ERK, extracellular signal-related kinase; JNK, Jun N-terminal kinase; LV, left ventricular; MAPK, mitogen-activated protein kinase; NO, nitric oxide; NOS, NO synthase; PE, phenylephrine; PECAM, platelet/EC adhesion molecule; RV, right ventricular; TG, transgenic.

Caveolae are 50–100-nm-long invaginations of the plasma membrane (1) that are important regulators of endocytosis (2) and signal transduction (3). There are three caveolin family members, caveolin-1 (Cav-1), which is predominantly expressed in adipocytes, vascular smooth muscle, endothelial cells (ECs), and fibroblasts; Cav-2, which is expressed in many cells that express Cav-1; and Cav-3, which is specifically expressed in skeletal, cardiac, and, to a lesser extent, in vascular smooth muscle. Cav-1 and -3 are essential for caveolae formation (4–6) in cells that express these isoforms, whereas Cav-2 is not absolutely required (7).

Recent insights into the physiological roles of caveolae/caveolins have been dissected in these genetically modified mice. Although Cav-1 and -3 are essential for caveolae formation, they are dispensable during vascular and organ development. The loss of Cav-1/caveolae, which is the primary isoform in the vascular system, results in dysregulation of nitric oxide (NO) synthesis, cell proliferation, enhanced vascular permeability, and pulmonary and cardiac functions, and it impairs liver regeneration (4, 5, 8–13). These studies validate the in vivo importance of caveolae and Cav-1 beyond cell-based studies that are largely hampered by operational definitions of biochemical fractions containing caveolins and the lack of specificity inherent in reagents that extract cholesterol from cells (14).

Vascular ECs constitute the surface monolayer of vasculature facing the blood and essential roles in the regulation of blood flow, blood pressure, and maintaining a selective permeability to macromolecules. EC barrier dysfunction results in various human diseases, including inflammation, tumor angiogenesis, and atherosclerosis. Indeed, the predominant phenotypes observed in Cav-1–deficient mice are vascular, cardiac, and pulmonary, and they may be caused by loss of caveolae in various cell types. Recent work from our group has shown that Cav-1 KO mice have impaired mechanotransduction, flow-dependent remodeling, and EC calcium influx via transient receptor potential

The online version of this article contains supplemental material.

The Journal of Experimental Medicine

channels; these effects are rescued by breeding global Cav-1 KO to EC-specific Cav-1 transgenic (TG) mice (15) to reconstitute Cav-1 (called Cav-1 RC) back into the endothelium (11, 16). We show that EC-specific Cav-1 reconstitution corrects the abnormal vasomotion in vessels and the cardiac and pulmonary abnormalities observed in Cav-1 KO mice, demonstrating that the diverse cardiovascular phenotypes in these mice are attributable to caveolae in the endothelium and not to other cell types that express Cav-1.

RESULTS

Generation of TG mice expressing EC Cav-1 on a Cav-1–deficient background

To assess the effects of Cav-1/caveolae on vascular, lung, and cardiac phenotypes, mice deficient in Cav-1 were bred to TG mice expressing Cav-1 in ECs alone, as previously reported (11, 16). Fig. 1 A documents Cav-1 protein expression in intrapulmonary arteries isolated from these mice. WT mice demonstrate the presence of Cav-1 (Fig. 1 A, left column, green channel) predominantly in the endothelium and lower levels in smooth muscle ($n = 5$; Fig. 1 A, top, Cav-1 alone; middle, labeling of smooth muscle α-actin [red] and nuclei [DAPI, blue]; bottom, merged images), whereas Cav-1 KO mice (middle column) lack Cav-1 immunostaining in both layers ($n = 5$). Reconstitution of Cav-1 into the endothelium generated by crossing Cav-1 KO to EC-specific Cav-1 TG mice reintroduces Cav-1 into the endothelium, but not into smooth muscle layers marked by α-smooth muscle actin staining ($n = 5$, right column). Insets show higher magnifications of images to emphasize correct targeting of the transgene.

Effects of EC-specific Cav-1 reconstitution on smooth muscle contractility and endothelium-dependent relaxation

Next, we examined how endothelium-specific Cav-1 reconstitution influences vasoreactivity, as there are biochemical and genetic data supporting a role of Cav-1 in regulating vascular function, including endothelial NO production and smooth muscle contraction. As shown in Fig. 1 (B and C), 0.01–10 μM phenylephrine (PE) and 15–65 mM KCl induced dose-dependent increases in isometric contractions in intrapulmonary arteries and responses to PE and KCl were reduced in vessels from Cav-1 KO mice. Interestingly, EC-specific Cav-1 RC was more responsive to PE than Cav-1 KO, but this did not occur with KCl as the agonist. Next, we examined acetylcholine (Ach)-induced endothelium-dependent relaxations in these vessels. As seen in Fig. 1 D, using PE as a contractile agonist, or in Fig. 1 E, using KCl as a contractile agonist, Ach-induced relaxations were augmented in Cav-1 KO vessels, and effects were normalized in Cav-1 RC mice.

Next, we measured cyclic guanosine monophosphate (cGMP) accumulation in intact vascular rings as a surrogate assay to quantify bioreactive NO production in intact pulmonary arterial rings (Fig. 1 F) and confirmed a significant increase in bioactive NO in Cav-1 KO arteries compared with

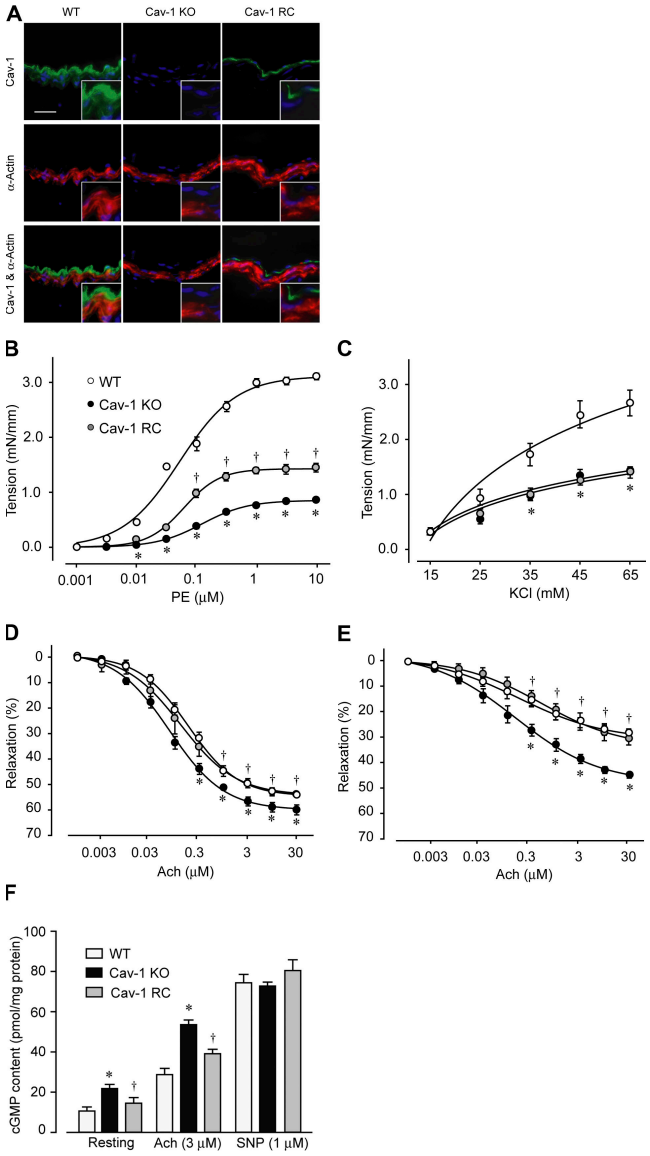

Figure 1. Characterization of pulmonary artery function in Cav-1 KO and Cav-1 RC mice. (A) Cav-1 (green) and smooth muscle α-actin (red) localization in WT, Cav-1 KO, and Cav-1 RC pulmonary arteries in cross sections by immunostaining (B and C). Bar, 20 μm. Insets show higher magnification images of section. Nuclei (blue) are detected via DAPI labeling. PE- (B) and high K^+–induced (C) contractions in WT, Cav-1 KO, and Cav-1 RC pulmonary arteries. Ach-induced relaxations in WT, Cav-1 KO, and Cav-1 RC pulmonary arteries. The arteries were precontracted with PE (D) or high K^+ (E), and Ach-induced relaxations were examined. (F) cGMP production in Cav WT, KO, and RC pulmonary arteries. *, $P < 0.05$, compared with WT vessels; †, $P < 0.05$, compared with Cav-1 KO vessels. Data are expressed as the mean ± the SEM.

WT arteries under resting and Ach-stimulated conditions (3 μM for 3 min). Again, EC-specific Cav-1 RC suppressed this increase in cGMP. In all of the strains, the sensitivity of the soluble guanylyl cyclase was normal because the increases in cGMP production in response to the NO donor sodium nitroprusside (1 μM for 3 min) were similar.

eNOS protein localization in endothelium and signaling to eNOS in Cav-1 KO is rescued in Cav-1 RC mice

Next, we used whole-mount immunofluorescent staining to examine the influence of Cav-1 KO and RC on endothelial NO synthase (eNOS) localization in intact endothelium lining intrapulmonary arteries. eNOS is typically colocalized on the Golgi complex and in Cav-1–positive plasmalemmal microdomains in vivo (11, 17, 18). Fig. 2 (A and B) demonstrates eNOS/Cav-1 (Fig. 2 A) and eNOS/GM130 (a peripheral membrane protein of Golgi complex) double-immunostaining (Fig. 2 B) in the endothelium of intact pulmonary arteries. WT and Cav-1 RC had similar levels of immunoreactive Cav-1 in ECs (n = 5 each; Fig. 2 B, middle row and left and right columns). Cav-1 KO vessels exhibited no Cav-1 immunoreactivity (n = 5). The pattern of eNOS labeling largely colocalized with GM 130 (Fig. 2 B, right) compared with WT and Cav-1 RC endothelium.

Next, we performed semiquantitative Western blotting for all caveolins in pulmonary arteries from WT, Cav-1 KO, and Cav-1 RC mice. As shown in Fig. 2 C, both Cav-1 and -2 levels were reduced in Cav-1 KO pulmonary arteries caused by the importance of Cav-1 in stabilizing Cav-2 levels (19, 20); effects were partially rescued in the Cav-1 RC vessels. However, Cav-3 and β-actin (as loading controls) levels were not different in the three genotypes of mice, nor were the protein levels of eNOS, HSP90, and the protein kinase Akt. However, the phosphorylation levels of eNOS (on the Akt and AMPK phosphorylation site S1177) and Akt (on S473) were increased in vessels from Cav-1 KO mice, indicating their activation (Fig. 2, C and D); this is an effect rescued in Cav-1 RC mice.

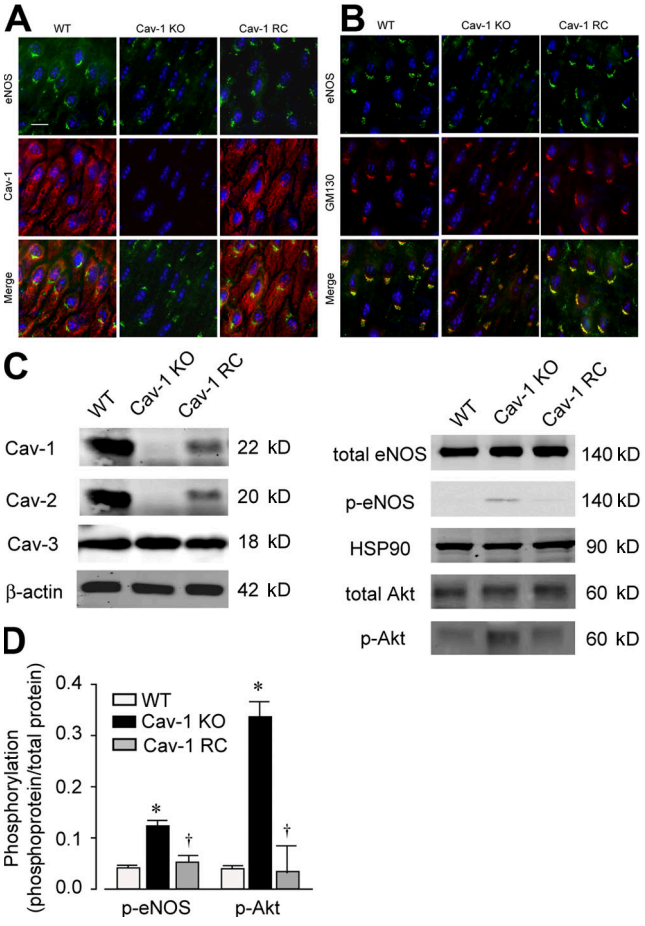

Figure 2. eNOS localization and activation in WT, Cav-1 KO, and Cav-1 RC pulmonary arteries. (A and B) eNOS (A and B, green), Cav-1 (A, red), and GM130 (B, red) expression in WT, Cav-1 KO, and Cav-1 RC pulmonary arteries in situ by whole-mount immunostaining. Bar, 100 nm. Nuclei (blue) are detected via DAPI labeling (C) caveolins, eNOS, HSP90; Akt protein expression and eNOS (Ser^{1179}) and Akt (Ser^{473}) phosphorylation in WT, Cav-1 KO, and Cav-1 RC pulmonary arteries. These blots are representative of four individual experiments. (D) Summary of eNOS and Akt phosphorylation-isolated vessels. Results are shown as phosphoprotein/total protein for eNOS and Akt, respectively. *, P, < 0.05, compared with WT vessels; †, P < 0.05, compared with Cav-1 KO vessels. Data are expressed as the mean ± the SEM.

Body weight and cardiac and pulmonary abnormalities are markedly improved in Cav-1 RC mice

In addition to vascular abnormalities, Cav-1 KO mice have lower body weight (8) and cardiac and pulmonary dysfunction. As shown in Table I, body weight was slightly lower in 20-wk-old Cav-1 KO compared with age-matched WT mice, and Cav-1 RC mice recovered this weight loss (n = 7–9). Cav-1 KO mice exhibit left ventricular (LV) and right ventricular (RV) cardiac hypertrophy (Fig. 3 A and Table I) using several measurements, including heart/body weight, RV/LV + septa, RV/body weight, and LV + septa/body weight, as previously reported (21). In addition, the diameter of the main coronary artery and coronary artery wall thicknesses was greater in Cav-1 KO mice, which is consistent with impaired remodeling of carotid arteries (11). EC-specific Cav-1 RC rescued these cardiac and vascular abnormalities to levels seen in age-matched WT mice. The lungs from Cav-1 KO mice were edematous with higher wet and dry weights and alveolar proliferation of the lower airways (Table I). These results are consistent with increased lung edema and cellularity in Cav-1 KO mice. Interestingly, EC-specific Cav-1 RC partially rescued the pulmonary defects.

Gross morphological changes of the hearts and lungs of Cav-1 KO mice: partial rescue of the phenotypes in Cav-1 RC mice

Fig. 3 demonstrates heart and lung morphology in all of the strains examined. As mentioned in Table I, Cav-1 KO displayed hypertrophy of both the right and left ventricles (Fig. 3 A) and greater coronary wall thickness (typical images; Fig. 3 B; Table I for quantification of coronary wall thickness). EC-specific Cav-1 RC improved these morphological endpoints. Similar to the heart, the lungs of Cav-1 KO mice exhibited cellular hyperproliferation in the alveolar area, bronchial epithelial layer (Fig. 3 B; indicated by B), and vascular layers (A indicates the artery, as seen in the typical images in Fig. 3 C and the summary of alveolar area in Table I). Interestingly,

Table I. Cardiac and pulmonary parameters in WT, Cav-1 KO, and Cav-1 RC mice

	10 wk			20 wk		
	WT	Cav-1 KO	Cav-1 RC	WT	Cav-1 KO	Cav-1 RC
Heart/body wt (mg/g)	4.60 ± 0.11	5.07 ± 0.06[b]	4.66 ± 0.07[a]	3.97 ± 0.09	5.07 ± 0.08[b]	3.98 ± 0.03[a]
RV/LV + septa (mg/mg)	0.25 ± 0.06	0.29 ± 0.10[b]	0.26 ± 0.07[a]	0.26 ± 0.06	0.32 ± 0.07[b]	0.26 ± 0.07[a]
RV/body wt (mg/g)	0.9 ± 0.03	1.15 ± 0.05[b]	1.00 ± 0.06[a]	0.81 ± 0.03	1.23 ± 0.03[b]	0.82 ± 0.02[a]
LV + septa/body wt (mg/g)	3.69 ± 0.09	3.92 ± 0.06[b]	3.72 ± 0.07[a]	3.16 ± 0.07	3.85 ± 0.12[b]	3.16 ± 0.08[a]
Coronary diameter (mm)	151.5 ± 2.5	157.0 ± 2.6	153.2 ± 1.8	152.4 ± 2.6	156.2 ± 4.5	149.8 ± 4.9
Coronary wall thickness (mm)	13.5 ± 0.4	20.5 ± 0.7[b]	14.4 ± 1.3[a]	12.9 ± 0.6	21.4 ± 1.6[b]	13.8 ± 1.7[a]
Body wt (g)	24.9 ± 0.4	24.9 ± 0.1	24.8 ± 0.3	34.1 ± 0.7	30.2 ± 1.4[b]	35.1 ± 0.9[a]
Lung wet wt (mg)	133.8 ± 2.8	158.2 ± 1.5[b]	144.8 ± 1.6[a]	160.2 ± 2.5	192.2 ± 1.0[b]	176.7 ± 2.4[a]
Lung dry wt (mg)	31.7 ± 0.2	43.0 ± 0.9[b]	37.0 ± 0.1[a]	41.2 ± 0.6	61.5 ± 0.9[b]	53.5 ± 0.7[a]
Lung water content (mg)	102.1 ± 2.4	115.2 ± 1.5[b]	107.8 ± 1.4[a]	119.0 ± 2.2	131.7 ± 1.1[b]	121.2 ± 1.9[a]
Alveolar area (%)	11.8 ± 0.7	32.9 ± 0.2[b]	21.9 ± 0.9[a]	12.0 ± 0.6	34.5 ± 1.3[b]	23.1 ± 1.4[a]

The results of the experiments are expressed as the means ± the SEM. $n = 5$–10 for all groups.
[a]Significantly different from Cav-1 KO; $P < 0.05$.
[b]Significantly different from WT; $P < 0.05$.

EC-specific Cav-1 RC partially rescued the bronchiole and alveolar hyperproliferation. Because the genetic rescue of these phenotypes was predicated on the proper targeting of the transgene to the endothelium in heart and lung, we examined immunoreactive Cav-1 in cardiac and pulmonary tissues from WT, Cav-1 KO, and Cav-1 RC mice. As seen in Fig. 3 D (heart) Cav-1 was expressed in cardiac vessels and capillaries (depicted in green channel, with α-smooth muscle actin in the red channel), was eliminated in Cav-1 KO, and was partially restored in Cav-1 RC hearts (arrowheads point out the presence of expressed transgene). In Fig. 3 E, Cav-1 is expressed in the epithelial layers of bronchi (indicated by B) and in endothelial/smooth muscle layers (marked by colabeling with α-smooth muscle actin) of adjacent pulmonary arteries (indicated by A, left column), patterns that are absent in Cav-1 KO tissue (middle column). Reexpression of Cav-1 in Cav-1 RC tissue was only detectable in the endothelial layer on arteries (indicated by A) and not in the bronchiole epithelium (Fig. 3 E, right column, arrowheads).

Correction of vascular leakage, pulmonary hypertension, and systemic blood pressure defects in Cav-1 RC mice

Because Cav-1 KO mice have enhanced basal vascular permeability, cardiac hypertrophy, and pulmonary hypertension, we quantified protein leakage, RV pressures, and systemic blood pressure in anesthetized WT, Cav-1 KO, and Cav-1 RC mice. To assess vascular permeability, we used Evans blue extravasation into the interstitium of tissues. As seen in Fig. 3 F, Evans blue extravasation into the heart and lungs of Cav-1 KO mice were increased compared with WT mice, effects rescued in Cav-1 RC mice. As shown in Fig. 3 G, baseline RV systolic pressure was elevated in Cav-1 KO, but reduced to WT levels in Cav-1 RC mice. Infusion of the positive inotrope dobutamine dose dependently increased RV systolic pressure in all strains, and the developed RV pressure was higher in Cav-1 KO hearts compared with the other strains. In addition, RV end-diastolic pressures were elevated in Cav-1 KO, but heart rates and positive dp/dt were not different (Fig. S1, available at http://www.jem.org/cgi/content/full/jem.20062340/DC1). In Cav-1 KO mice, systemic blood pressure was lower than WT and Cav-1 RC mice (Fig. 3 H). To assess whether this lower systemic arterial pressure was from enhanced eNOS activation in Cav-1 KO or not, the effect of the NOS inhibitor *N*-nitro-L-arginine methyl ester on blood pressure as examined. Infusion of 10 mg/kg *N*-nitro-L-arginine methyl ester increased systemic blood pressure to an equal extent in all strains and normalized the difference in basal pressure seen in Cav-1 KO mice, suggesting that the lower systemic pressure is dependent on eNOS hyperactivation in Cav-1 KO.

Regulation of signaling in hearts and lungs from Cav-1 KO and TG mice

Cav-1 and -2 are coexpressed in most types, including endothelial and smooth muscle cells, whereas Cav-3 is enriched in muscle cells, especially in cardiac myocytes. Thus, the relative levels of caveolins in heart and lung homogenates (compared with three loading controls [β-actin, eNOS, and HSP90]) were assessed in all strains (Fig. 4 A, right, top three gels). Cardiac and pulmonary tissue contained all three Cav isoforms, with more Cav-3 in the heart and more Cav-1 and -2 in the lung. The loss of Cav-1 reduced Cav-1 and -2 levels in both tissues. In both heart and lung, reconstitution of Cav-1 to EC rescued Cav-1 and -2 protein expression, albeit to a lesser extent in heart, which is likely caused by the higher abundance of EC in lungs. The absence or presence of Cav-1 expression did not affect the levels of total eNOS, HSP90, Akt, p42/44 extracellular signal-related kinase (ERK), p38 mitogen-activated protein kinase (MAPK), and Jun N-terminal kinase (JNK) proteins (Fig. 4 A), but did selectively

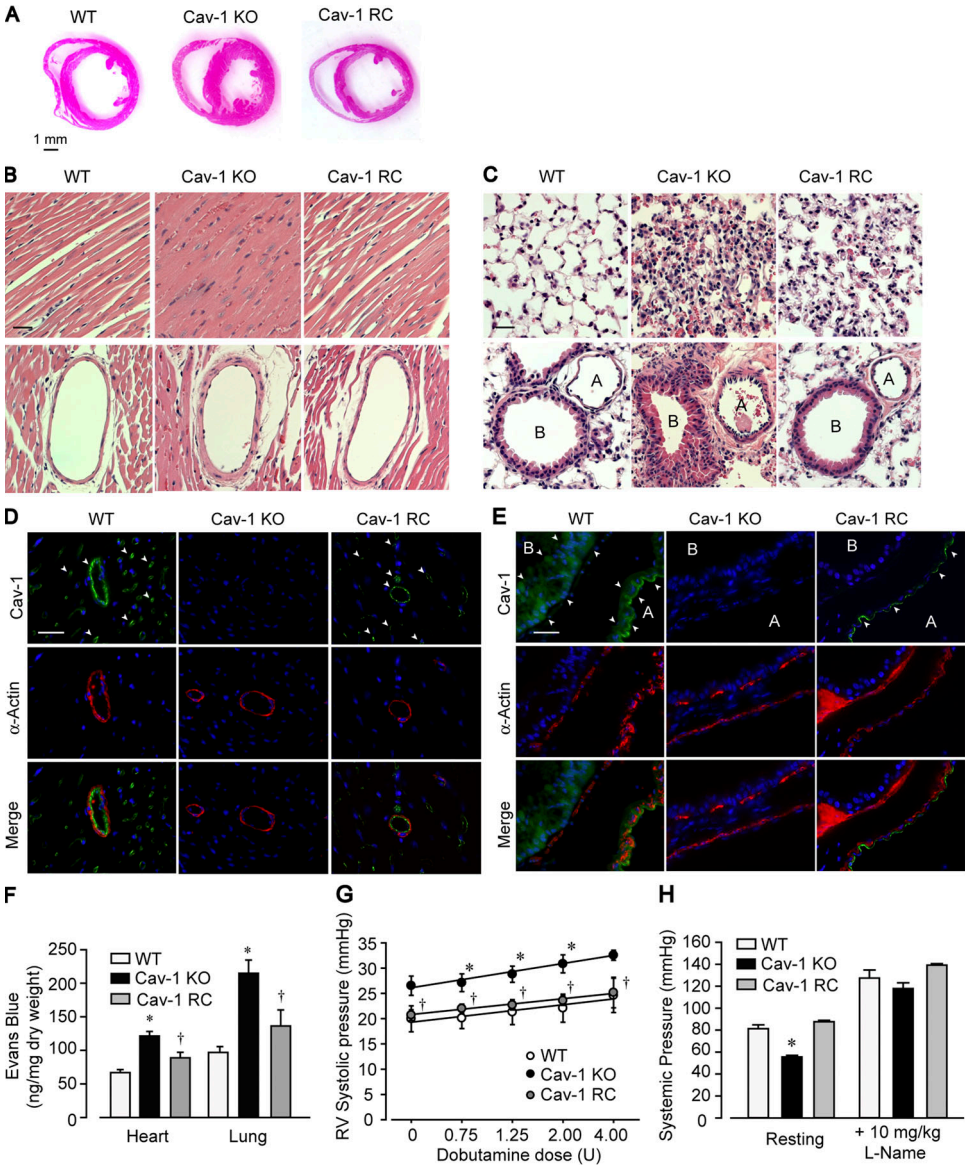

Figure 3. Heart and lung morphology and hemodynamics in WT, Cav-1 KO, and Cav-1 RC mice. (A–C) Hearts and lungs were stained with hematoxylin and eosin. (A) Low-magnification pictures of heart slices. (B) Cardiac muscle (top) and wall thickness of main coronary arteries (bottom). (C) Alveolar area (top) and large bronchioles (B, bottom) and arteries (A) in lung. (D and E). Cav-1 expression in WT, Cav-1 KO, and Cav-1 RC hearts (D) and lungs (E). Arrows delineate Cav-1 expression in Cav-1 RC mice. Nuclei (blue) are detected via DAPI labeling. These figures are representative of 4–6 experiments. Basal vascular permeability (F), right ventricle (RV) systolic pressure under nonstimulated and dobutamine-stimulated conditions (G), and mean systemic blood pressure (G) in Cav-1 WT, KO, and RC pulmonary arteries. Data are the means ± the SEM. n = 4–6 mice per group. *, $P < 0.05$, compared with WT vessels; †, $P < 0.05$, compared with Cav-1 KO vessels. Bars: (A) 1 mm; (B–E) 200 μm.

modulate the phosphorylation state of some of these proteins. In Cav-1 KO hearts, Akt (Ser^{473}) phosphorylation and p42/44 (Thr^{202}/Tyr^{204}) phosphorylation were elevated, but the phosphorylation states of p38 MAPK and JNK were not (Fig. 4 B). Interestingly, in hearts from Cav-1 RC mice, activation of Akt and p42/44 ERK were restored to WT levels. The increased phospho-Akt and -ERK can also be detected in the main coronary arteries (Fig. 4, C and D) and, to a much lesser extent, in cardiac fibroblasts (Fig. S2, available at http://www.jem.org/cgi/content/full/jem.20062340/DC1) of Cav-1 KO mice. In Cav-1 KO lungs, there was an increase in immunoreactive pAkt (Ser^{473})- and p42/44 (Thr^{202}/Tyr^{204}) in pulmonary arteries (Fig. 4, E and F, top) and epithelium (middle and bottom). In lung extracts of Cav-1 KO mice, there was elevated p38 MAPK (Thr^{180}/Tyr^{182}) hyperphosphorylation, with no change in phospho-JNK levels. In contrast to the heart extracts, EC-specific Cav-1 RC mice only partially (phospho-Akt) or did not correct the elevated activation of p42/44 ERK or p38 MAPK in lung extracts.

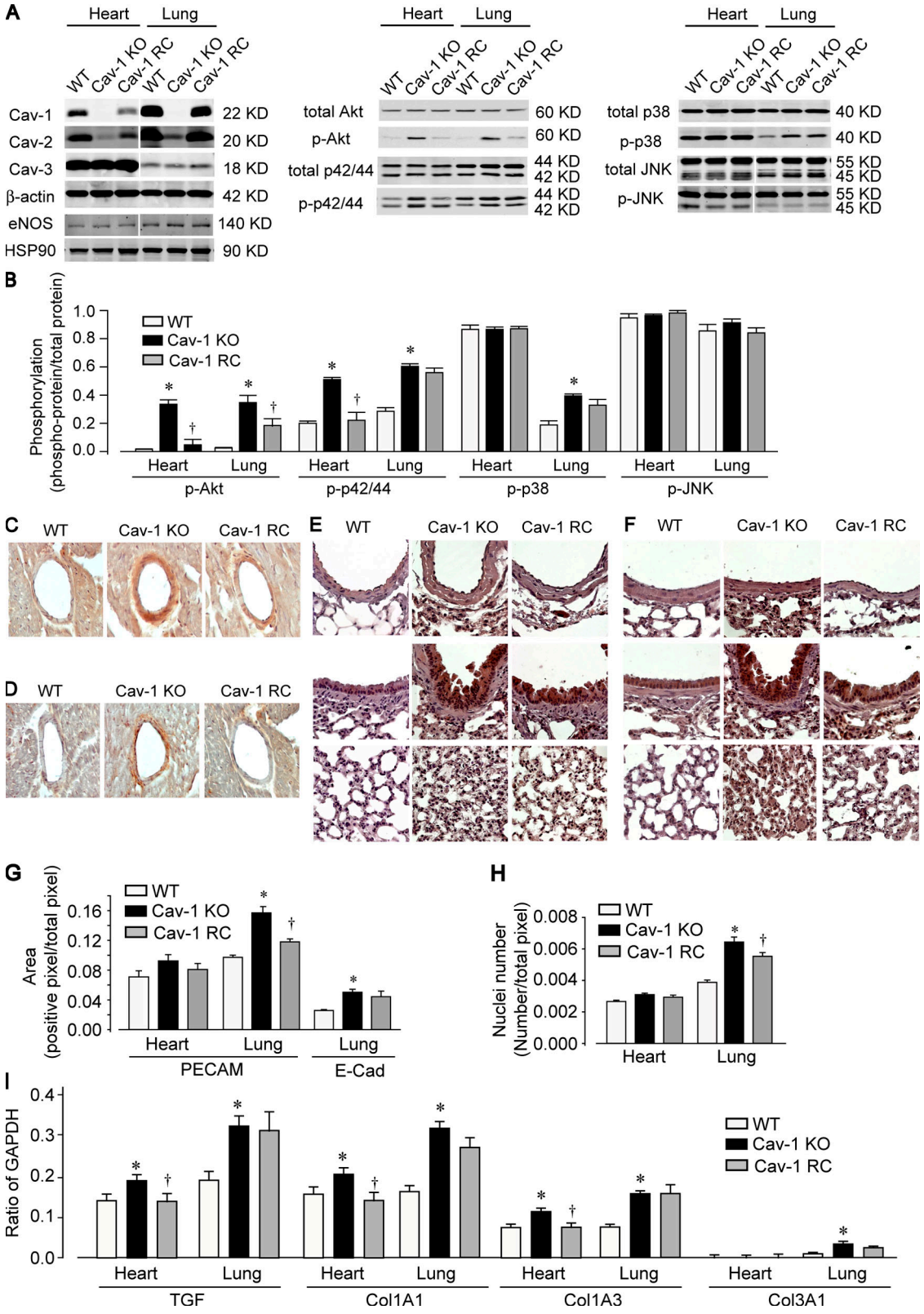

Figure 4. Enhanced Akt and p42/44 ERK phosphorylation and fibrogenic gene expression in hearts and lungs of WT, Cav-1 KO, and Cav-1 RC mice. (A and B) Total caveolins, eNOS, HSP90, Akt, p42/44, p38, and JNK protein expression and phosphor-Akt (Ser^{473}), p42/44 (Thr^{202}/Tyr^{204}), p38 (Thr^{180}/Tyr^{182}) in tissue extracts. (A) Typical Western blots from six individual experiments; (B) the summary of these experiments by quantitative imaging. Akt (Ser^{473}) phosphorylation (C) and p42/44 (Thr^{202}/Tyr^{204}) phosphorylation (D) in main coronary arteries of the three strains of mice, respectively. Akt (Ser^{473})

Increased signaling in Cav-1 KO mice is linked to hyperproliferation and collagen synthesis

To examine the link between the loss of Cav-1, activation of signaling pathways, and cell proliferation, sections from hearts and lungs were immunolabeled and quantified for the expression of the EC marker platelet/EC adhesion molecule-1 (PECAM-1) and the epithelial cell marker E-cadherin (E-cad; Fig. 4 G and Fig. S3, available at http://www.jem.org/cgi/content/full/jem.20062340/DC1). In the heart, the number of PECAM-1–positive cells did not change in the three strains, but in the lung, Cav-1 KO lungs had increased numbers of ECs and epithelial cells per area of section analyzed. The increase in PECAM-1–positive, but not E-cad–positive, cells in the lung was reduced in Cav-1 RC mice. Similar results were obtained using Western blotting for the EC marker VE cadherin and for E-cad (unpublished data). The data quantifying ECs and epithelial cells were recapitulated by counting the total number of DAPI-stained nuclei per area in heart and lung sections (Fig. 4 H).

Finally, because of the alveolar and septal changes observed in the lungs of Cav-1 KO mice and the recent study showing that patients with idiopathic pulmonary fibrosis exhibit a marked decrease in Cav-1 expression linked to up-regulation of TGF-β signaling (22), we examined the expression of TGF-β1 and the interstitial collagens (I and III) via RT-PCR. As seen in Fig. 4 I, the expression of TGF-β1, type I collagen α 1 chain (Col1A1), α 3 chain (Col1A3), and type III collagen α 1 chain (Col3A1) were increased in Cav-1 KO hearts and lungs. The increase in TGF-β1 and Col1A3 expression were rescued in the hearts by the transgene, whereas Col1A1 and Col3A1 were partially rescued in the lung.

DISCUSSION

The lack of embryonic lethality in Cav-1 KO mice has allowed investigators to test the importance of this protein and its corresponding organelle in several postnatal functions. Several groups have independently generated Cav-1 KO mice, and they have reported that Cav-1/caveolae KO mice possess clear and reproducible vascular, cardiac, and pulmonary phenotypes (4, 5, 10). These phenotypes, driven by the global loss of Cav-1, may be caused by the loss of the gene from many cells that express it, including ECs, smooth muscle cells, adipocytes, fibroblasts, and epithelial cells. Our findings argue that the major vascular, cardiac, and pulmonary phenotypes in Cav-1 KO are largely caused by the loss of caveolae in the endothelium lining the vasculature of these organs, supporting the concept that endothelial Cav-1 can regulate paracrine functions governing remodeling of cardiac and pulmonary tissue.

There are biochemical and genetic data supporting a role for Cav-1 as a negative regulator of agonist-mediated eNOS activation (4, 5, 10, 12, 23–25). Consistent with these reports, eNOS hyperactivation was observed in Cav-1 KO pulmonary arteries as assessed by vascular relaxation experiments, cGMP measurements, Western blotting for activated Akt (S473 phosphorylation) and eNOS (S1177 phosphorylation), and in vivo hemodynamic studies, phenotypes were completely rescued in Cav-1 RC mice. In addition, we show that Cav-1 deficiency impaired PE- and high K^+–induced vascular smooth muscle isometric tension generation in isolated intrapulmonary arteries. Although contractile responses to PE, but not KCl, were improved in vessels from EC-specific Cav-1 RC mice, the overall defect in vascular smooth muscle function was not restored, suggesting that this phenotype is EC independent and dependent on Cav-1 in vascular smooth muscle. This is consistent with reports in Cav-1 KO mice, showing impairment in calcium signaling (spontaneous transient oscillatory currents and capacitive calcium entry; reference [16]) and contractility in vascular smooth muscle from isolated microvessels (5). In Cav-1 KO vessels, the levels of Cav-3 did not change, suggesting that Cav-3 was not responsible for this contractile defect in smooth muscle.

In the heart, Cav-1 is expressed in cardiac endothelium and fibroblasts, but not in cardiomyocytes, where Cav-3 is the major isoform. In the lung, Cav-1 and -2 are expressed in the endothelium, most epithelial cells, and fibroblasts, and Cav-3 is present in airway and vascular smooth muscle. However, despite the paucity of Cav-1 in cardiomyocytes, Cav-1 KO mice display cardiac hypertrophy, pulmonary hypertension, and pulmonary hyperplasia associated with hyperactivation of the p42/p44 ERK–MAPK and Akt pathways, as well as cellular hyperproliferation and increased collagen gene expression in the lung. In respect to the cardiac phenotypes, using echocardiography and gated MRI, hearts from Cav-1 KO mice exhibited concentric LV hypertrophy and dilated RV hypertrophy secondary to pulmonary hypertension (21). Another independent study using echocardiography alone showed both dilated LV and RV dimensions in hearts of Cav-1 KO mice; the dilation was caused by pulmonary hypertension (10). Our data supports the role of the endothelium in these phenotypes because EC-specific reconstitution of Cav-1 lowered pulmonary pressure and normalized RV dilation and LV hypertrophy. However, the most direct evidence for the independent role of Cav-1 on cardiopulmonary function versus pulmonary hyperplasia and alveolar thickening is supported by data documenting that Cav-2 KO mice (which retain Cav-1 expression) do not have cardiac hypertrophy or pulmonary hypertension, but do exhibit pulmonary hyperplasia (7). More importantly, we show that both cardiac

phosphorylation (E) and p42/44 (Thr^{202}/Tyr^{204}) phosphorylation (F) in pulmonary arteries (top) and lung parenchyma (middle showing large airway and bottom showing alveoli). Photos are representative from four separate experiments. Quantitative analysis of PECAM-1 and E-cad (G) and total nuclei (H) in hearts and lungs of WT, Cav-1 KO, and Cav-1 RC mice. Expression of TGF-β1, and interstitial collagen genes (I) by RT-PCR (compared with GAPDH) in total RNA isolated from hearts and lungs of WT, Cav-1 KO, and Cav-1 RC mice. Data are the means ± the SEM. $n = 4$ mice per group.

morphometry and pulmonary hypertension are rescued in Cav-1 RC mice, strongly supporting a role for endothelial Cav-1 as the major cell type contribution to LV hypertrophy and RV remodeling, secondary to pulmonary hypertension. In the context of pulmonary hyperplasia and lung remodeling, the beneficial effect of the Cav-1 transgene may be caused by stabilizing Cav-2 in the endothelium, which then leads to a partial genetic rescue of the phenotype, which is consistent with a role of Cav-2 regulating alveolar hyperplasia. This could be directly tested by EC-specific reexpression of Cav-2. Interestingly in the hearts and lungs of Cav-1 KO mice, gene expression of TGF-β1 and interstitial collagens I and III were elevated, effects rescued in the hearts, but not lungs, which is consistent with the idea that abnormal TGF-β signaling may contribute to these phenotypes.

Another interesting finding in our study was that vascular and cardiac abnormalities in Cav-1 KO mice were largely rescued in Cav-1 RC mice, but the lung abnormalities were only partially rescued. In the lung, the reintroduction of EC-specific Cav-1 stabilized Cav-2 levels and rescued pulmonary hypertension, and the enhanced lung permeability and edema, but only partially rescued the increased alveolar area, endothelial (PECAM-1 staining), and alveolar (E-cad staining) hyperplasia in Cav-1 KO mice. In lung extracts from Cav-1 KO mice, the basal levels of pAkt, p42/p44 ERK, and p38 MAPK activation were elevated compared with lungs from WT mice, and in Cav-1 RC mice, only lung pAkt activation was rescued. This suggests that a majority of the cells that contribute to increased Akt activity in Cav-1 KO are of vascular origin, whereas activation of ERK and p38 MAPK occurred primarily in epithelia or fibroblasts. In lung tissue, EC and epithelial cells are the major cells expressing Cav-1 protein and epithelial Akt and p42/44 ERK were highly phosphorylated in Cav-1 KO lungs. EC-specific Cav-1 RC did not affect epithelial Cav-1 deficiency, and its proliferation associated with activation of Akt- and p42/44 ERK. Given recent evidence that a decrease in Cav-1 is associated with increased fibrosis (22, 26), we examined genes linked to fibrosis in the three strains. Interestingly, in the hearts and lungs of Cav-1 KO mice, gene expression of TGF-β1 and interstitial collagens I and III were elevated; these effects were rescued in the hearts, but not the lungs, which is consistent with the idea that abnormal TGF-β signaling may contribute to these phenotypes.

The idea that Cav-1/caveolae microdomains are important for signal transmission from the cell surface originated from work in the Ras-ERK, G-protein, and eNOS pathways, but has extended to many other signaling pathways (3). Because this work was, for the most part, performed in vitro with purified proteins and relied on fractionation procedures and the enrichment of Cav-1 and caveolae and the sensitivity of signaling pathways to agents that disrupt cholesterol synthesis, it was met with much skepticism. Work in Cav-1 KO mice has convincingly shown that Cav-1 can negatively regulate ERK and eNOS activity; however, based on this study, Cav-1 also regulates Akt and p38 MAPK activation in a cell-specific manner and strongly impacts cardiac size and pulmonary functions. These data support the idea that caveolae are vital membrane microdomains that cluster or integrate signaling in vivo, as well as in vitro.

In conclusion, the generation of EC-specific Cav-1 RC mice and correction of several phenotypes supports the idea that endothelial Cav-1 plays a central role in blood vessel, pulmonary, and cardiac functions. Whether the loss of Cav-1 in endothelium leads to constitutive activation of all signaling in ECs (eNOS, ERK, Akt, and p38 MAPK) or if the loss of Cav-1 in endothelium exerts paracrine effects on adjacent cardiac and pulmonary parenchyma, leading to the observed cardiac and pulmonary phenotypes, is not known and will be the focus of future studies. Additional studies generating cell-specific knockouts of Cav-1 and -2 or TG reexpression of these isoforms in non-ECs in the global knockout background will strengthen the idea that caveolins exert cell-specific roles in signaling and function.

MATERIALS AND METHODS

Generation of Cav-1–deficient and EC-specific Cav-1 RC animals. Endothelial-specific Cav-1 TG mice carrying canine Cav-1 transgene under the preproendothelin-1 promoter (15) were crossed with F5 generation Cav-1–deficient mice (5), as previously described (11). All mice were genotyped for the presence of endogenous murine Cav-1, the presence of neomycin cassette, and the presence of canine Cav-1 transgene using specific PCR primers. Male mice (10 and 20 wk old) were used for the experiments. After anesthesia with 100 mg/kg ketamine/xylazine i.m. and PBS perfusion from RV under physiological pressure (~20 mmHg), all tissues (pulmonary artery, lung, and heart) were dissected and used for each experiments. All animal procedures were approved by the Yale Institutional Animal Care and Use Committee.

Tissue processing. Hearts and lungs were removed en bloc. In some experiments, lungs were blotted dry, weighed, and put on aluminum foil to dry overnight in the oven; dry weight of tissue is recorded the next day. The heart RV and LV plus septum (LV + septa) were separated and weighed.

Immunofluorescence and immunohistochemistry. After dissection, intrapulmonary arteries, hearts, and lungs (from 10-wk-old mice) were fixed with 4% paraformaldehyde for 10 min at 4°C, and then dehydrated in 15% sucrose overnight at 4°C. The vessels were then embedded in OCT (Sakura) and flash-frozen in a liquid nitrogen–cooled isopentane bath. 5-μm sections were blocked with 3% normal goat serum. For immunofluorescence studies, the slides were incubated with rabbit anti-Cav-1 antibody (BD Transduction Laboratories), mouse anti–α-smooth muscle actin antibody Cy3 conjugate (Sigma-Aldrich), rat anti–VE-cadherin antibody (BD PharMingen), and rat anti–E-cad antibody (1:200 dilution; 4°C for 12 h; Zymed Laboratories). Alexa Fluor 488 anti–rat/–rabbit IgG (Invitrogen) was used as secondary antibody (1:500 dilution; at room temperature for 1 h). For immunohistochemistry, slides were probed with rabbit anti–phospho-Akt (Ser^{473}) antibody (Cell Signaling Technology) and anti–phospho-p42/44 (Thr^{202}/Tyr^{204}) antibody (1:200 dilution; 4°C for 12 h; Cell Signaling Technology). After the incubation with biotinylated anti–rabbit IgG (Jackson ImmunoResearch Laboratories), we probed the samples using the Nova Red staining kit (Vector Laboratories).

Whole-mount staining. The intrapulmonary arteries (from 10-wk-old mice) were fixed with 4% paraformaldehyde (4°C for 10 min), permeabilized with 0.3% Triton X-100 PBS (at room temperature for 30 min), and blocked by 3% normal goat serum containing PBS (at room temperature for

30 min). The arteries were probed with rabbit anti–Cav-1 antibody (BD Transduction Laboratories), mouse anti-eNOS antibody (BD Bioscience), rabbit anti-eNOS antibody (BD Transduction Laboratories), and mouse anti-GM130 antibody (BD Transduction Laboratories; 1:200 dilution; 4°C for 12 h). Alexa Fluor 488/568 anti–rabbit IgG and 488/568 anti–mouse IgG (Invitrogen) were used as secondary antibodies (1:500 dilution; room temperature for 1 h).

Isometric tension in vessels. Intrapulmonary arteries were dissected from male mice (10 wk old) and cut into 3-mm-long segments. The rings are suspended by two tungsten wires mounted in a vessel myograph system (Danish Myotechnologies). The arteries were bathed in oxygenated Krebs buffer and submitted to a resting tension of 3 mN. After equilibration, concentration-response curves for high-potassium (KCl) and PE were generated. To study vasodilator responses, the rings were preconstricted with submaximal concentrations of KCl (35 mM) and PE (1 μM), and Ach (10 nM–30 μM) was added at the plateau of the PE-induced contraction.

Measurement of cGMP content. After the incubation in oxygenated Krebs buffer and stimulations with Ach or sodium nitroprusside, vascular rings were immediately frozen in liquid nitrogen, homogenized in 6% trichloroacetic acid solution, and centrifuged at 2,000 *g* for 15 min at 4°C, as previously described (15). The supernatants were applied to a cGMP enzyme–immunoassay system (GE Healthcare), and pellets were used to determine protein content. cGMP contents are expressed as picomole/milligram protein content.

Western blotting. Equal amounts (60 μg) of protein from the total homogenates of the intrapulmonary artery, lung, and heart were used for SDS-PAGE, followed by Western blot analysis. The membranes were probed with rabbit anti–Cav-1 antibody (BD Transduction Laboratories), mouse anti–Cav-2 antibody (BD Transduction Laboratories), mouse anti–Cav-3 antibody (BD Transduction Laboratories), mouse anti–β-actin antibody (Sigma-Aldrich), mouse anti-eNOS antibody (BD Transduction Laboratories), rabbit anti–phospho-eNOS (Ser^{1179}) antibody (BD Transduction Laboratories), mouse anti-HSP90 antibody (BD Transduction Laboratories), rabbit anti-Akt antibody (Cell Signaling Technology), rabbit anti–phospho-Akt (Ser^{473}) antibody (Cell Signaling Technology), rabbit anti-p42/44 antibody (Cell Signaling Technology), rabbit anti–phospho-p42/44 (Thr^{202}/Tyr^{204}) antibody (Cell Signaling Technology), rabbit anti-p38 antibody (Cell Signaling Technology), rabbit anti–phospho-p38 (Thr^{180}/Tyr^{182}) antibody (Cell Signaling Technology), rabbit anti-JNK antibody (Cell Signaling Technology), and rabbit anti–phospho-JNK (Thr^{183}/Tyr^{185}) antibody (Cell Signaling Technology) at dilutions ranging from 1:200 to 1:1,000.

Hemodynamic studies. Mice were anesthetized by i.m. intraperitoneal ketamine/xylazine injection. Mice were intubated and placed on positive-pressure ventilation, and light anesthesia was maintained by inhaled isoflurane. The left common jugular vein was cannulated with polyethylene tubing (PE 10) and a 1.9-French transducer-tipped catheter (Millar, Inc.) was advanced into the right ventricle via the right common jugular vein. RV pressures, including high-fidelity positive and negative dp/dt, were measured under basal conditions and during intravenous infusion of graduated doses of dobutamine. Data were recorded by using Mac Lab software and were analyzed by using the Heartbeat program. Systemic blood pressures were measured from carotid arterial cannulas fitted with a pressure transducer.

Modified Miles assay. Mice were anesthetized with 100 mg/kg ketamine/xylazine i.m., and a catheter was introduced into the left jugular vein for administration of 30 mg/kg Evans blue (Sigma-Aldrich). After 30 min, the animals were killed and perfused with warmed PBS, and the tissues were dissected, blotted dry, and put on aluminum foil to dry overnight in the oven; dry weight of tissue was recorded the next day. The Evans blue content of the tissue was evaluated by extraction with 500 μl–1 ml of formamide for 24 h at 55°C and measured spectrophotometrically at 630 nm. Results were compared with a standard curve of Evans blue in formamide

Statistical analysis. The results of the experiments are expressed as the means ± the SEM. Statistical evaluation of the data was performed by analysis of variance, followed by the Tukey posttest for comparison between groups using Prism 3.0. A value of $P < 0.05$ was regarded as statistically significant.

Online supplemental material. Fig. S1 shows cardiac function in Cav-1 WT, KO, and RC mice. Fig. S2 shows phospho-42/44 phosphorylation in Cav-1 WT, KO, and RC heart interstitial fibroblasts. Fig. S3 shows EC and epithelial cell proliferation in Cav-1 WT, KO, and RC heart and lung. The online version of this article is available at http://www.jem.org/cgi/content/full/jem.20062340/DC1.

This work was supported from National Institutes of Health grants R01 HL64793, R01 HL 61371, R01 HL 57665, and P01 HL 70295 and the National Heart, Lung, and Blood Institute Yale Proteomics contract N01-HV-28186 to W.C. Sessa.

The authors have no conflicting financial interests.

Submitted: 7 November 2006
Accepted: 16 August 2007

REFERENCES

1. Bruns, R.R., and G.E. Palade. 1968. Studies on blood capillaries. I. General organization of blood capillaries in muscle. *J. Cell Biol.* 37: 244–276.
2. Schnitzer, J.E., J. Liu, and P. Oh. 1995. Endothelial caveolae have the molecular transport machinery for vesicle budding, docking, and fusion including VAMP, NSF, SNAP, annexins, and GTPases. *J. Biol. Chem.* 270:14399–14404.
3. Smart, E.J., G.A. Graf, M.A. McNiven, W.C. Sessa, J.A. Engelman, P.E. Scherer, T. Okamoto, and M.P. Lisanti. 1999. Caveolins, liquid-ordered domains, and signal transduction. *Mol. Cell. Biol.* 19:7289–7304.
4. Razani, B., J.A. Engelman, X.B. Wang, W. Schubert, X.L. Zhang, C.B. Marks, F. Macaluso, R.G. Russell, M. Li, R.G. Pestell, et al. 2001. Caveolin-1 null mice are viable but show evidence of hyperproliferative and vascular abnormalities. *J. Biol. Chem.* 276:38121–38138.
5. Drab, M., P. Verkade, M. Elger, M. Kasper, M. Lohn, B. Lauterbach, J. Menne, C. Lindschau, F. Mende, F.C. Luft, et al. 2001. Loss of caveolae, vascular dysfunction, and pulmonary defects in caveolin-1 gene-disrupted mice. *Science.* 293:2449–2452.
6. Galbiati, F., J.A. Engelman, D. Volonte, X.L. Zhang, C. Minetti, M. Li, H. Hou Jr., B. Kneitz, W. Edelmann, and M.P. Lisanti. 2001. Caveolin-3 null mice show a loss of caveolae, changes in the microdomain distribution of the dystrophin-glycoprotein complex, and t-tubule abnormalities. *J. Biol. Chem.* 276:21425–21433.
7. Razani, B., X.B. Wang, J.A. Engelman, M. Battista, G. Lagaud, X.L. Zhang, B. Kneitz, H. Hou Jr., G.J. Christ, W. Edelmann, and M.P. Lisanti. 2002. Caveolin-2-deficient mice show evidence of severe pulmonary dysfunction without disruption of caveolae. *Mol. Cell. Biol.* 22:2329–2344.
8. Razani, B., T.P. Combs, X.B. Wang, P.G. Frank, D.S. Park, R.G. Russell, M. Li, B. Tang, L.A. Jelicks, P.E. Scherer, and M.P. Lisanti. 2002. Caveolin-1-deficient mice are lean, resistant to diet-induced obesity, and show hypertriglyceridemia with adipocyte abnormalities. *J. Biol. Chem.* 277:8635–8647.
9. Schubert, W., P.G. Frank, S.E. Woodman, H. Hyogo, D.E. Cohen, C.W. Chow, and M.P. Lisanti. 2002. Microvascular hyperpermeability in caveolin-1 (−/−) knock-out mice. Treatment with a specific nitric-oxide synthase inhibitor, L-name, restores normal microvascular permeability in Cav-1 null mice. *J. Biol. Chem.* 277:40091–40098.
10. Zhao, Y.Y., Y. Liu, R.V. Stan, L. Fan, Y. Gu, N. Dalton, P.H. Chu, K. Peterson, J. Ross Jr., and K.R. Chien. 2002. Defects in caveolin-1 cause dilated cardiomyopathy and pulmonary hypertension in knockout mice. *Proc. Natl. Acad. Sci. USA.* 99:11375–11380.
11. Yu, J., S. Bergaya, T. Murata, I.F. Alp, M.P. Bauer, M.I. Lin, M. Drab, T.V. Kurzchalia, R.V. Stan, and W.C. Sessa. 2006. Direct evidence for the role of caveolin-1 and caveolae in mechanotransduction and remodeling of blood vessels. *J. Clin. Invest.* 116:1284–1291.

12. Wunderlich, C., K. Schober, S.A. Lange, M. Drab, R.C. Braun-Dullaeus, M. Kasper, C. Schwencke, A. Schmeisser, and R.H. Strasser. 2006. Disruption of caveolin-1 leads to enhanced nitrosative stress and severe systolic and diastolic heart failure. *Biochem. Biophys. Res. Commun.* 340:702–708.
13. Fernandez, M.A., C. Albor, M. Ingelmo-Torres, S.J. Nixon, C. Ferguson, T. Kurzchalia, F. Tebar, C. Enrich, R.G. Parton, and A. Pol. 2006. Caveolin-1 is essential for liver regeneration. *Science.* 313:1628–1632.
14. Gratton, J.P., P. Bernatchez, and W.C. Sessa. 2004. Caveolae and caveolins in the cardiovascular system. *Circ. Res.* 94:1408–1417.
15. Bauer, P.M., J. Yu, Y. Chen, R. Hickey, P.N. Bernatchez, R. Looft-Wilson, Y. Huang, F. Giordano, R.V. Stan, and W.C. Sessa. 2005. Endothelial-specific expression of caveolin-1 impairs microvascular permeability and angiogenesis. *Proc. Natl. Acad. Sci. USA.* 102:204–209.
16. Murata, T., M.I. Lin, R.V. Stan, P.M. Bauer, J. Yu, and W.C. Sessa. 2007. Genetic evidence supporting caveolae microdomain regulation of calcium entry in endothelial cells. *J. Biol. Chem.* 282:16631–16643.
17. Cheng, C., R. van Haperen, M. de Waard, L.C. van Damme, D. Tempel, L. Hanemaaijer, G.W. van Cappellen, J. Bos, C.J. Slager, D.J. Duncker, et al. 2005. Shear stress affects the intracellular distribution of eNOS: direct demonstration by a novel in vivo technique. *Blood.* 106:3691–3698.
18. van Haperen, R., C. Cheng, B.M. Mees, E. van Deel, M. de Waard, L.C. van Damme, T. van Gent, T. van Aken, R. Krams, D.J. Duncker, and R. de Crom. 2003. Functional expression of endothelial nitric oxide synthase fused to green fluorescent protein in transgenic mice. *Am. J. Pathol.* 163:1677–1686.
19. Mora, R., V.L. Bonilha, A. Marmorstein, P.E. Scherer, D. Brown, M.P. Lisanti, and E. Rodriguez-Boulan. 1999. Caveolin-2 localizes to the Golgi complex but redistributes to plasma membrane, caveolae, and rafts when co-expressed with caveolin-1. *J. Biol. Chem.* 274:25708–25717.
20. Parolini, I., M. Sargiacomo, F. Galbiati, G. Rizzo, F. Grignani, J.A. Engelman, T. Okamoto, T. Ikezu, P.E. Scherer, R. Mora, et al. 1999. Expression of caveolin-1 is required for the transport of caveolin-2 to the plasma membrane. Retention of caveolin-2 at the level of the Golgi complex. *J. Biol. Chem.* 274:25718–25725.
21. Cohen, A.W., D.S. Park, S.E. Woodman, T.M. Williams, M. Chandra, J. Shirani, A. Pereira de Souza, R.N. Kitsis, R.G. Russell, L.M. Weiss, et al. 2003. Caveolin-1 null mice develop cardiac hypertrophy with hyperactivation of p42/44 MAP kinase in cardiac fibroblasts. *Am. J. Physiol. Cell Physiol.* 284:C457–C474.
22. Wang, X.M., Y. Zhang, H.P. Kim, Z. Zhou, C.A. Feghali-Bostwick, F. Liu, E. Ifedigbo, X. Xu, T.D. Oury, N. Kaminski, and A.M. Choi. 2006. Caveolin-1: a critical regulator of lung fibrosis in idiopathic pulmonary fibrosis. *J. Exp. Med.* 203:2895–2906.
23. Michel, J.B., O. Feron, D. Sacks, and T. Michel. 1997. Reciprocal regulation of endothelial nitric-oxide synthase by Ca2+-calmodulin and caveolin. *J. Biol. Chem.* 272:15583–15586.
24. Garcia-Cardena, G., P. Martasek, B.S. Masters, P.M. Skidd, J. Couet, S. Li, M.P. Lisanti, and W.C. Sessa. 1997. Dissecting the interaction between nitric oxide synthase (NOS) and caveolin. Functional significance of the nos caveolin binding domain in vivo. *J. Biol. Chem.* 272:25437–25440.
25. Bucci, M., J.P. Gratton, R.D. Rudic, L. Acevedo, F. Roviezzo, G. Cirino, and W.C. Sessa. 2000. In vivo delivery of the caveolin-1 scaffolding domain inhibits nitric oxide synthesis and reduces inflammation. *Nat. Med.* 6:1362–1367.
26. Razani, B., X.L. Zhang, M. Bitzer, G. von Gersdorff, E.P. Bottinger, and M.P. Lisanti. 2001. Caveolin-1 regulates transforming growth factor (TGF)-beta/SMAD signaling through an interaction with the TGF-beta type I receptor. *J. Biol. Chem.* 276:6727–6738.